Thermochimica Acta 494 (2009) 129–135

Contents lists available at ScienceDirect

Thermochimica Acta

journal homepage: www.elsevier.com/locate/tca

Effect of wide range of heating rate on the crystallization kinetic parameters of $Se_{77}Te_{20}Sb_3$ glass

M. Abu El-Oyoun*

Physics Department, Faculty of Science, Taibah University, PO Box 30002, Madina, Saudi Arabia

ARTICLE INFO

Article history:
Received 28 February 2009
Received in revised form 2 May 2009
Accepted 8 May 2009
Available online 20 May 2009

PACS:
6470 P
6140
6140 D

Keywords:
$Se_{77}Te_{20}Sb_3$ chalcogenide glass
Crystallization kinetics
Activation energy
DSC
Isoconversional methods

ABSTRACT

The kinetic parameters of glassy $Se_{77}Te_{20}Sb_3$ under non-isothermal conditions are analyzed by the model-fitting and model-free approaches. Differential scanning calorimetry (DSC) technique was used to study the kinetics of amorphous to crystalline transformation for $Se_{77}Te_{20}Sb_3$ glass using a wide range of heating rates (4–90 K/min). The analysis of the present data shows that the activation energy of crystallization is not constant but varies with the degree of conversion and hence with temperature. The reaction model that may describe the crystallization process of the $Se_{77}Te_{20}Sb_3$ glass is model A2 (Avrami–Erofeev with $n=2$) for heating rates 4–30 K/min. While, the reaction model A3/2 (Avrami–Erofeev with $n=1.5$) is a proper model that may describe crystallization process of the present glass for higher heating rates (35–90 K/min). The crystallization mechanisms examined using the local Avrami exponents indicate that one mechanism (two-dimensional growth) is responsible for the crystallization process for heating rates (4–30 K/min) and two mechanisms (one- and two-dimensional growth) are working simultaneously during the amorphous–crystalline transformation of glassy $Se_{77}Te_{20}Sb_3$ for higher heating rates (35–90 K/min). A good agreement between the experimental and the reconstructed (α–T) curves has been achieved. The transformation from amorphous to crystalline phase in glassy $Se_{77}Te_{20}Sb_3$ demonstrates complex multi-step involving several processes.

1. Introduction

Kinetic studies are always connected with the concept of activation energy. The activation energy of the glass crystallization is associated with nucleation and growth processes. Studies of the crystallization of a glass upon heating can be performed in several different ways and the crystallization process can be interpreted in terms of several theoretical models [1–7]. The differential scanning calorimetry (DSC) is one of the tools to study the crystallization kinetics, which has been widely discussed in the literature [8–12]. Thermally activated transformations in the solid state can be investigated by isothermal or non-isothermal experiments [13–17].

Addition of trace elements in amorphous alloys is one of the most effective methods for exploiting new amorphous alloys or improving their properties [18]. As stated by Huang et al. [18], the element to be added has similar chemical properties to one of the alloy component elements, or is significantly different from the alloy elements in atomic radius, which makes the atomic packing become denser, and the glass-forming ability (GFA), thermal stability, tensile strength and other mechanical properties are improved [18–21]. The Se–Te alloys are found to be useful in practical application. From a technological point of view these glasses should be thermally stable with time and temperature during use [22]. However, thermal instability leading to crystallization is found to be one of the drawback of these alloys and hence several attempts have been made to improve the stability of Se–Te by the addition of third element. As stated by Saxena [22], element like antimony, which belongs to V group is found to improve the stability as well as photoconductivity. The kinetic of crystallization for amorphous Se–Te–Sb glass was studied using the DSC technique under non-isothermal conditions by many authors [23–25].

The kinetic transformation of amorphous gives information relative to the stability and applicability of these materials. One of the common experimental techniques used for the kinetic studies is the differential scanning calorimetry (DSC). The DSC data are analyzed with the help of the isoconversional (model-free) and model-fitting methods to get information about the kinetic parameters such as activation energy, E, pre-exponential factor, A and reaction model, $g(\alpha)$ [26,27].

Bonastre et al. [28] have pointed that a detailed knowledge of the temperature dependence of nucleation and crystalline growth is essential for nano-materials design and to control their microstructure. Furthermore, in technical applications, the thermal stability of amorphous alloys is a problem of fundamental interest to determine the useful working temperature ranges [28].

* Tel.: +966 509275263; fax: +966 48454770.
E-mail address: moha4202@yahoo.com.

0040-6031/$ – see front matter © 2009 Elsevier B.V. All rights reserved.
doi:10.1016/j.tca.2009.05.006

In the present work, the crystallization kinetic of amorphous $Se_{77}Te_{20}Sb_3$ glass is studied using the DSC technique under non-isothermal conditions. The dependence of the crystallization kinetic parameters on the extent of conversion, α, for a wide range of heating rates (β = 4–90 K/min) is discussed.

2. Experimental procedure

Bulk material was prepared by the well-established melt-quench technique. The high purity (99.999%) Se, Te and Sb in appropriate at.% proportion were weighed in a quartz glass ampoule (12 mm diameter). The contents of the ampoule were sealed under a vacuum of 10^{-4} Torr (0.01 Pa) and heated at around 950 K for 24 h. During the melt process, the tube was frequently shaken to homogenize the resulting alloy. The melt was quenched in water at 273 K to obtain the glassy state.

The differential scanning calorimetry (DSC) was carried out on approximately 3 mg quantities of powder samples using a Shimadzu DSC-60 with sensitivity of ±10 μW. The accuracy of the heat flow is ±0.01 mW and the temperature precision as determined by the microprocessor of the thermal analyzer is ±0.1 K. The heating rates were varied from 4 to 90 K/min under dry nitrogen supplied at the rate 50 ml/min. To minimize the temperature gradient the samples were well granulated to form uniform fine powder and spread as thinly as possible on the bottom of the sample pan. Temperature and enthalpy calibration were checked with indium at heating rate 10 K/min (T_m = 156.6 °C, ΔH_m = 28.55 J/g) as standard material supplied by Shimadzu. This calibration was checked at different heating rates.

3. Results and discussion

Fig. 1 shows the DSC curves at different heating rates, β = 4–90 K/min for the $Se_{77}Te_{20}Sb_3$ chalcogenide glass. The DSC curves show two characteristic effects. The glass transition temperature, T_g, as defined by the endothermic change in the DSC

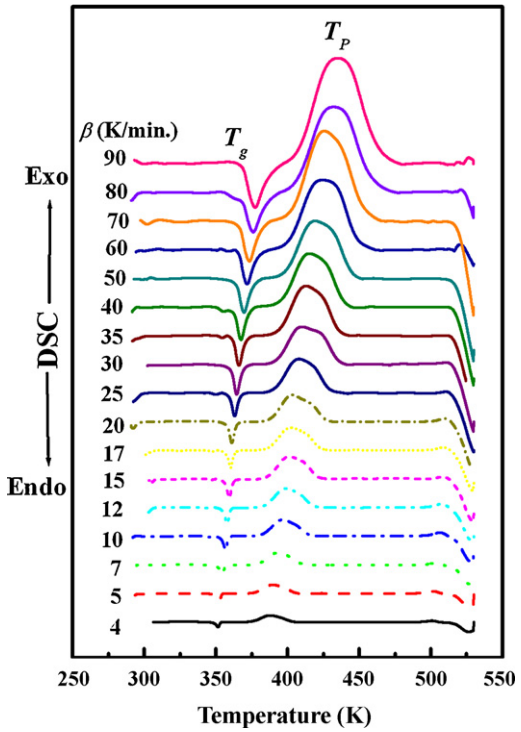

Fig. 1. Typical DSC trace of glassy $Se_{77}Te_{20}Sb_3$ for β = 4–90 K/min.

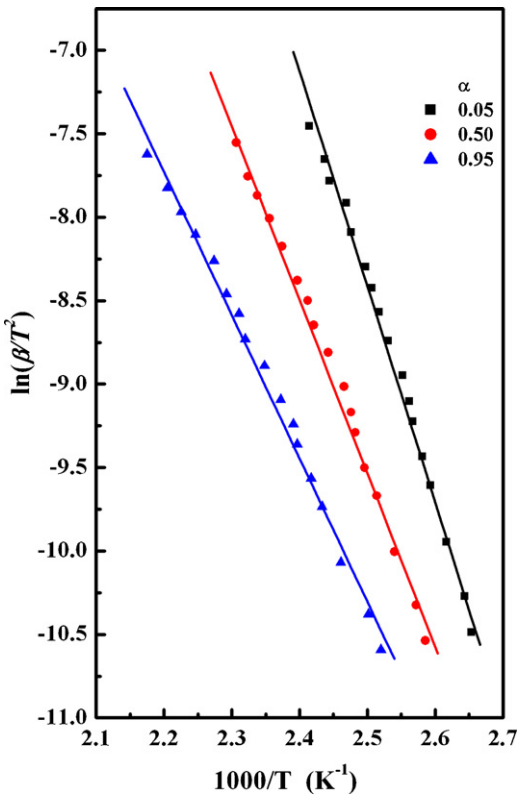

Fig. 2. A plot of $\ln(\beta/T^2)$ vs. $1000/T$ for a = 0.05, 0.50 and 0.95. The straight lines are fit to Kissinger equation.

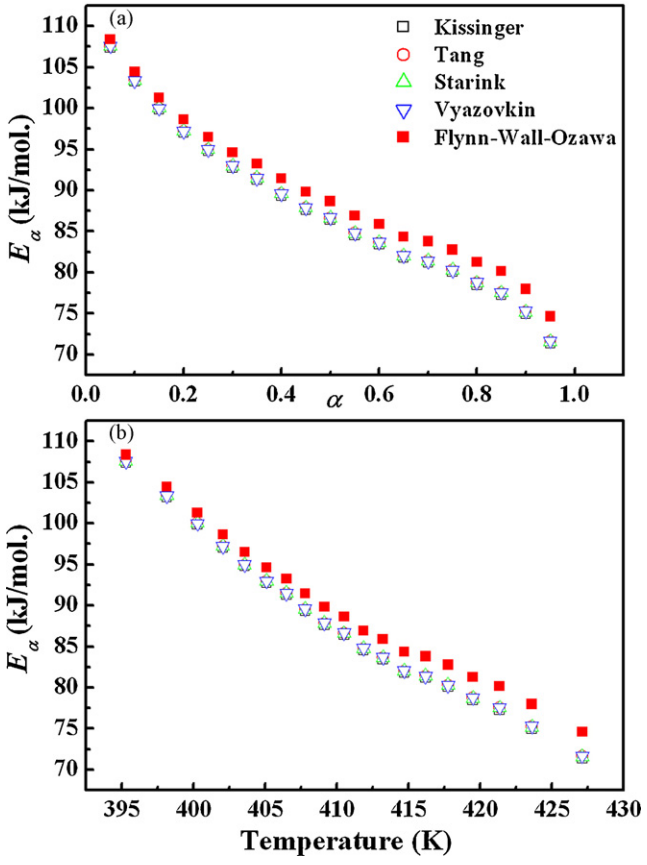

Fig. 3. Dependence of the activation energy for crystallization, E_α on: (a) the volume of the crystallization fraction, α and (b) the temperature, T, for different model-free methods.

trace indicates a large change of viscosity, marking a transformation from amorphous solid phase to supercooled liquid state. The second characteristic is the exothermic peak temperature, T_p, which represents the temperature at the maximum crystallization rate. This behaviour is typical for a glass–crystalline transformation. The two characteristic temperatures shifted to higher temperatures with increasing the heating rate.

Vyazovkin [29], Kissinger–Akahira–Sunose [1,4,30], Starink [6,31], Tang [32] and Flynn–Wall–Ozawa [2,3] isoconversional methods were used to investigate the variation of the effective activation energy with extent of crystallization and hence with temperature. The observed dependence of the effective activation energy on the heating rate can be attributed to the possible variation of E_α with temperature [5,8,9]. The above isoconversional methods can be summarized as follow:

(1) Vyazovkin method [29]:

$$\Omega = \sum_{i=1}^{n} \sum_{j \neq i}^{n} \frac{I(E_\alpha, T_{\alpha i})\beta_j}{I(E_\alpha, T_{\alpha j})\beta_i} \tag{1}$$

where n is the number of heating rates. The activation energy can be determined at any particular value of α by finding the value of E_α which minimizes the objective function Ω.

where the integral temperature $I(E, T)$ is given by:

$$I(E, T) = \int_{T_{\alpha-\Delta\alpha}}^{T_\alpha} \exp\left(-\frac{E}{RT}\right) \mathrm{d}T \tag{2}$$

The temperature integral, $I(E, T)$, was evaluated using an approximation suggested by Gorbachev [33]:

$$\int_0^T \exp\left(-\frac{E}{RT}\right) \mathrm{d}T = \frac{RT^2}{E}\left(\frac{1}{1+(2RT/E)}\right)\exp\left(-\frac{E}{RT}\right) \tag{3}$$

The minimization procedure is repeated for each value of α to find the dependence of E_α on α.

(2) The Kissinger–Akahira–Sunose (KAS) method [1,4,30]:

$$\ln\left(\frac{\beta_i}{T_{\alpha i}^2}\right) = C_K(\alpha) - \frac{E_\alpha}{RT_{\alpha i}} \tag{4}$$

(3) The Starink method [6,31]:

$$\ln\left(\frac{\beta_i}{T_{\alpha i}^{1.92}}\right) = C_S(\alpha) - 1.0008\frac{E_\alpha}{RT_{\alpha i}} \tag{5}$$

(4) The Tang method [32]:

$$\ln\left(\frac{\beta_i}{T_{\alpha i}^{1.894661}}\right) = C_T(\alpha) - 1.00145033\frac{E_\alpha}{RT_{\alpha i}}. \tag{6}$$

(5) The Flynn–Wall–Ozawa (FWO) method, suggested independently by Flynn and Wall [2] and Ozawa [3]. This method is given by:

$$\ln\ \beta_i = C_W(\alpha) - 1.0518\frac{E_\alpha}{RT_{\alpha i}}. \tag{7}$$

As stated above, Vyazovkin, KAS, Starink, Tang and FWO isoconversional methods were used to investigate the variation of the effective activation energy with extent of crystallization and hence with temperature. Fig. 2 displays an example of estimating the activation energy at constant extent of conversion $\alpha = 0.05$, 0.50 and 0.95 by plotting $\ln(\beta/T^2)$ against $1000/T$ using KAS method. The slopes of the straight lines (with a correlation coefficient of 0.9969) shown in the figure are used to calculate the activation energy for that particular α value. This procedure is repeated for other values of α.

Fig. 3 shows the variation of the crystallization activation energy, E_α, as a function of both α, Fig. 3a, and temperature, Fig. 3b, according to all the above isoconversional methods. Vyazovkin, KAS, Starink and Tang methods give similar values of E_α, while FWO method gives values of E_α higher than the values obtained by the other isoconversional methods. This close agreement between Vyazovkin, KAS, Starink and Tang isoconversional methods was also reported by many authors [8,25,34–38].

The analysis of the present data based on all isoconversional methods used shows that the activation energy of crystalliza-

Table 1
Algebraic expressions of $f(\alpha)$ and $g(\alpha)$ for the reaction models considered in the present work [16].

No.	Symbol	Reaction model	$f(\alpha)$	$g(\alpha)$
Power law				
1	P1	$n = 1/4$	$4\alpha^{3/4}$	$\alpha^{1/4}$
2	P2	$n = 1/3$	$3\alpha^{2/3}$	$\alpha^{1/3}$
3	P3	$n = 1/2$	$2\alpha^{1/2}$	$\alpha^{1/2}$
4	P4	$n = 3/2$	$2/3\alpha^{-1/2}$	$\alpha^{3/2}$
Phase-boundary controlled reaction				
5	R1	Contracting linear	1	α
6	R2	Contracting area	$2(1-\alpha)^{1/2}$	$[1-(1-\alpha)^{1/2}]$
7	R3	Contracting volume	$3(1-\alpha)^{2/3}$	$[1-(1-\alpha)^{1/3}]$
Chemical reaction				
8	F1	First-order (Mampel)	$(1-\alpha)$	$-\ln(1-\alpha)$
9	F3/2	Three-halves order	$(1-\alpha)^{3/2}$	$2[(1-\alpha)^{-1/2}-1]$
10	F2	Second-order	$(1-\alpha)^2$	$[(1-\alpha)^{-1}-1]$
11	F3	Third-order	$(1-\alpha)^3$	$(1/2)[(1-\alpha)^{-2}-1]$
Avrami–Erofeev				
12	A3/2	$n = 1.5$	$(3/2)(1-\alpha)[-\ln(1-\alpha)]^{1/3}$	$[-\ln(1-\alpha)]^{2/3}$
13	A2	$n = 2$	$2(1-\alpha)[-\ln(1-\alpha)]^{1/2}$	$[-\ln(1-\alpha)]^{1/2}$
14	A3	$n = 3$	$3(1-\alpha)[-\ln(1-\alpha)]^{2/3}$	$[-\ln(1-\alpha)]^{1/3}$
15	A4	$n = 4$	$4(1-\alpha)[-\ln(1-\alpha)]^{3/4}$	$[-\ln(1-\alpha)]^{1/4}$
Diffusion				
16	D1	One-dimensional diffusion	$1/2\alpha$	α^2
17	D2	Two-dimensional diffusion	$1/[-\ln(1-\alpha)]$	$[(1-\alpha)\ln(1-\alpha)+\alpha]$
18	D3	Three-dimensional diffusion (Jander equation)	$3(1-\alpha)^{1/3}/2[(1-\alpha)^{-1/3}-1]$	$[1-(1-\alpha)^{1/3}]^2$
19	D4	Three-dimensional diffusion (Ginstling–Brounshtein)	$3/2[(1-\alpha)^{-1/3}-1]$	$(1-2\alpha/3)-(1-\alpha)^{2/3}$

Table 2
The values of a, b, K_{iso}, T_{iso}, T_r and R_C, using Kennedy–Clark method (Eq. (8)), obtained by all reaction models listed in Table 1 for $Se_{77}Te_{20}Sb_3$ glass (for $\alpha = 0.05$–0.95).

β (K/min)	a (min^{-1})	b (mol/kJ)	K_{iso} (min^{-1})	T_{iso} (K)	T_r (K)	R_C
4	−3.5715	0.3065	0.0281	392.43	377–398	0.99972
5	−3.3383	0.3047	0.0355	394.75	378–400	0.99971
7	−3.0427	0.3017	0.0477	398.67	381–405	0.99965
10	−2.7252	0.2986	0.0656	402.81	384–410	0.99961
12	−2.5770	0.2968	0.0760	405.25	386–413	0.99958
15	−2.3543	0.2945	0.0950	408.42	388–415	0.99954
17	−2.2435	0.2937	0.1061	409.53	389–417	0.99953
20	−2.1005	0.2919	0.1224	412.06	390–420	0.99947
25	−1.8885	0.2892	0.1513	415.90	393–424	0.99947
30	−1.7312	0.2862	0.1771	420.26	395–429	0.99935
35	−1.5936	0.2856	0.2032	421.15	397–430	0.99940
40	−1.4714	0.2837	0.2296	423.97	398–433	0.99935
50	−1.2863	0.2806	0.2763	428.65	402–438	0.99929
60	−1.1220	0.2780	0.3256	432.66	403–443	0.99914
70	−0.9927	0.2759	0.3706	435.95	407–447	0.99917
80	−0.8806	0.2727	0.4145	441.07	408–453	0.99898
90	−0.6246	0.2686	0.5355	447.80	412–457	0.99882

tion is not constant but varies with the degree of conversion and hence with temperature. So, the transformation from amorphous to crystalline cannot be described by a single-step mechanism. The transformation demonstrates complex multi-step involving several processes of growth with different activation energies and mechanisms [34,35,39,40].

For non-isothermal experiments, model-fitting involves fitting different models to (α–T) curves to determine E_α and A_α [34,41]. One of these models proposed by Kennedy–Clark method [42], which is given by the following expression:

$$\ln\left[\frac{\beta g(\alpha)}{T - T_0}\right] = \ln(A) - \frac{E}{RT} \tag{8}$$

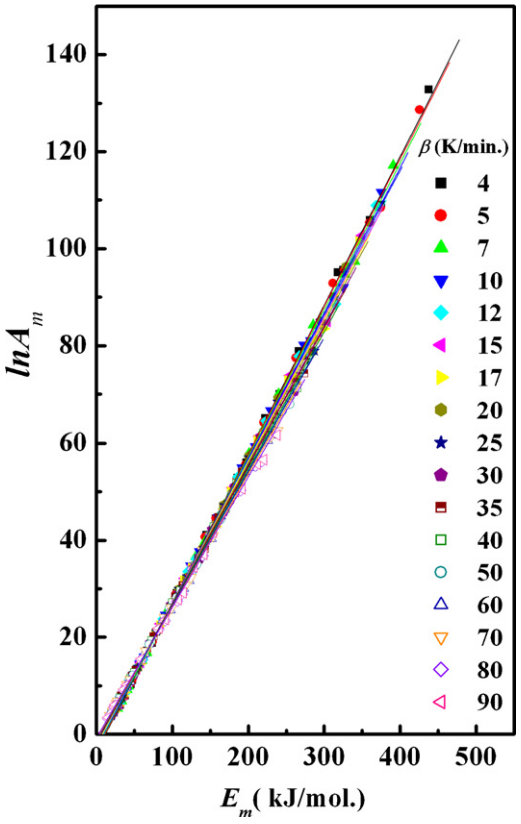

Fig. 4. The isokinetics relationships using Kennedy–Clark method for $\beta = 4$–90 K/min.

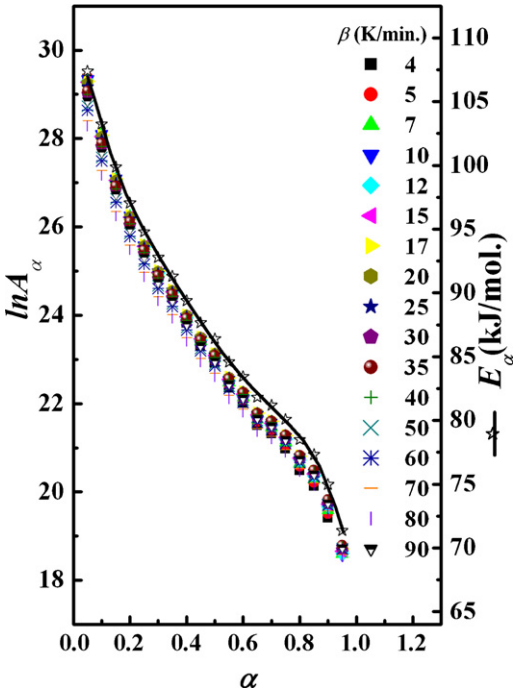

Fig. 5. Dependence of $\ln A_\alpha$ on the volume of the crystallization fraction, α, $\beta = 4$–90 K/min.

where T_0 is the initial temperature of the reaction. Plotting $\ln[\beta g(\alpha)/(T - T_0)]$ vs. $1/T$ gives a straight line of slope $(-E/R)$ and the intercept $\ln A$ for different reaction models of $g(\alpha)$. The most common reaction models used to describe solid state reactions is listed in Table 1 [16].

Vyazovkin [39] has stated that the model-free kinetics turn the experimental values of A_α and $g(\alpha)$ or $f(\alpha)$ into unnecessary kinetic

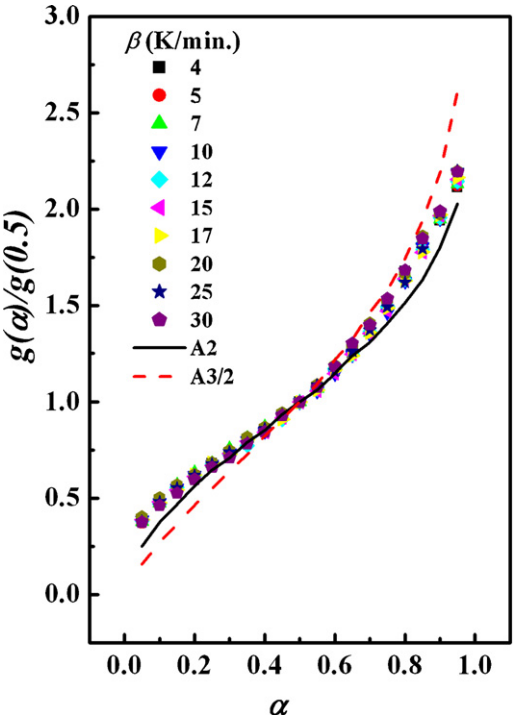

Fig. 6. The dependence of the experimental $g(\alpha)/g(0.5)$ on the volume of the crystallization fraction, α, for $\beta = 4$–30 K/min. The solid line represents the theoretical models.

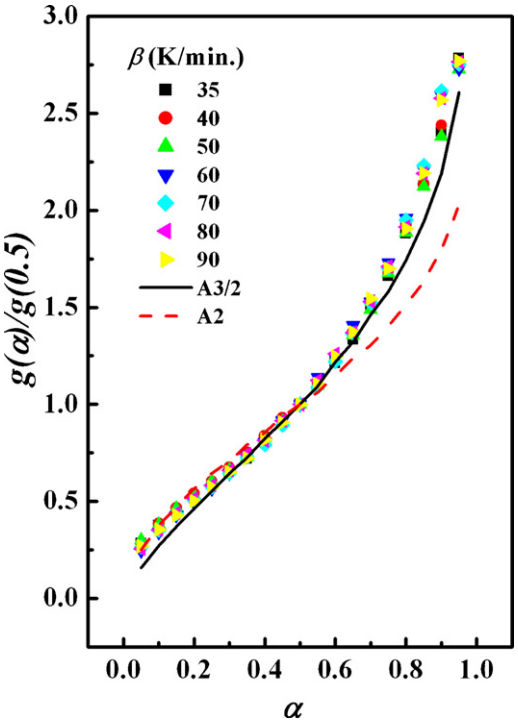

Fig. 7. The dependence of the experimental $g(\alpha)/g(0.5)$ on the volume of the crystallization fraction, α, for β = 35–90 K/min. The solid line represents the theoretical models.

entities. Once the experimental values of A_α are known, one can evaluate the reaction mode that fits to the experimental data. The values of $\ln A_m$ and E_m of different reaction models are related linearly, which are known as "compensation effect" and typically obey the following form [34,39]:

$$\ln A_m = a + bE_m \quad (9)$$

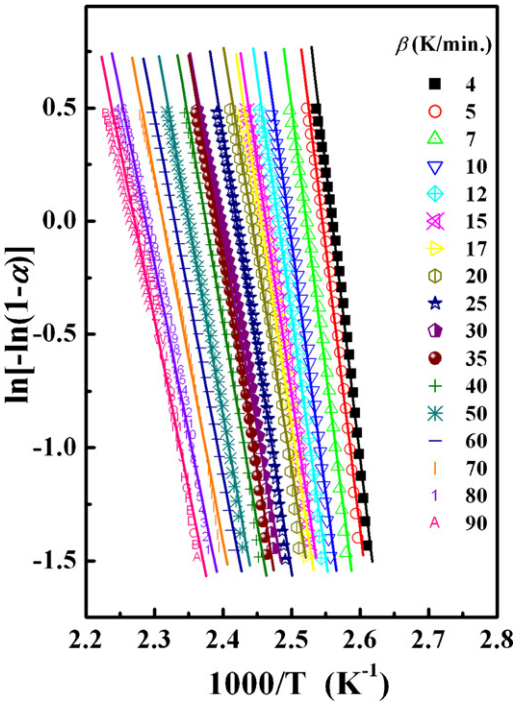

Fig. 8. $\ln[-\ln(1-\alpha)]$ vs. $1000/T$ plots at all heating rates for glassy $Se_{77}Te_{20}Sb_3$.

where a is an artificial isokinetic rate constant ($a = \ln K_{iso}$) and constant b is given by ($b = 1/RT_{iso}$) where K_{iso} is an artificial isokinetic rate constant and T_{iso} is an artificial isokinetic temperature. The subscript m in Eq. (9) refers to one of possible reaction models $g(\alpha)$ or $f(\alpha)$. In the present work, the kinetic parameters are determined by fitting the experimental (α–T) curve obtained at a single heating rate to the model-fitting proposed by Kennedy–Clark (Eq. (8)).

The values of (a, b) and hence (K_{iso}, T_{iso}) could be obtained by plotting $\ln A_m$ vs. E_m for β = 4–90 K/min in the range of α (0.05–0.95) using all reaction models listed in Table 1. In addition to the above parameters the T_r and R_C could be calculated also, where T_r is the experimental temperature range of each β and R_C is correlation coefficient of the linear relationships shown in Fig. 4. From Table 2, it is clear that both K_{iso} and T_{iso} increase with β, as well as the value of T_{iso} lies in the experimental temperature range, T_r, for each β. If the value of T_{iso} lies out of the range of T_r for any heating rate it means that the models chosen are not proper models to describe the crystallization process of the present glass.

Once the correlation parameters (a and b) have been evaluated, Table 2, E_α values are substituted for E_m in Eq. (9) to estimate the corresponding $\ln A_\alpha$ values and obtaining the dependence of $\ln A_\alpha$ on α. As stated by Vyazovkin et al. [43,44] the above procedure could be applied for multi-step reactions that involving several processes as it is, originally, applied to a single-step process. Fig. 5 shows the dependence of $\ln A_\alpha$ on α for each heating rate. It is clear from this figure that this dependence ($\ln A_\alpha$ vs. α) is typically as the dependence of E_α on α. Once the experimental values of E_α and $\ln A_\alpha$ have been obtained one can reconstruct the reaction model numerically [34,39].

By comparing the obtained experimental values of E_α and $\ln A_\alpha$ with that obtained from each model listed in Table 1, then

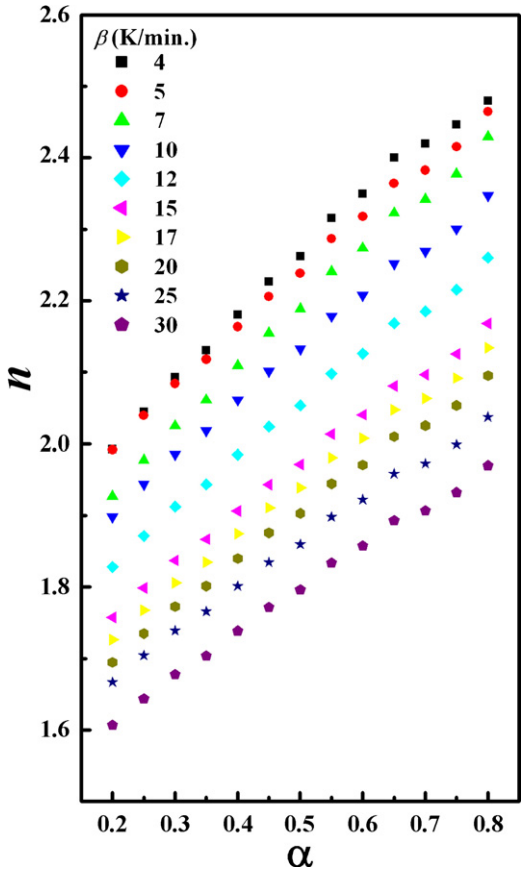

Fig. 9. The variation of local Avrami exponent, $n(\alpha)$, on the volume of the crystallization fraction, α, for β = 4–30 K/min.

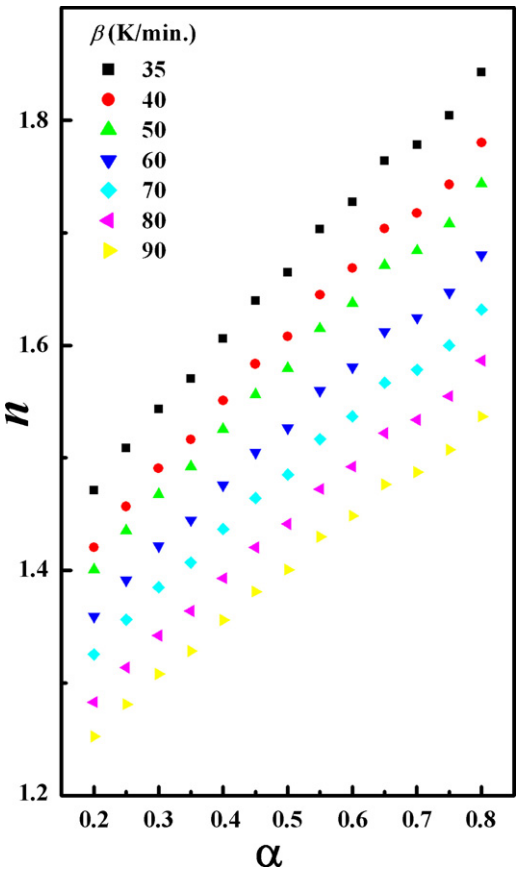

Fig. 10. The variation of local Avrami exponent, $n(\alpha)$, on the volume of the crystallization fraction, α, for $\beta = 35$–90 K/min.

the suitable reaction model $g(\alpha)$ will be chosen to describe the crystallization process of $Se_{77}Te_{20}Sb_3$ glass. For example, the values of kinetic parameters (E_α and E_m) and ($\ln A_\alpha$ and $\ln A_m$) are (107.39, 105.72 kJ/mol.) and (29.35, 29.13) for $\beta = 4$ K/min, respectively, at $\alpha = 0.05$. The values of these parameters, for $\beta = 35$ K/min at $\alpha = 0.9$, are (74.98, 75.21 kJ/mol.) and (20.49, 20.17), respectively. For $\beta = 90$ K/min the values of (E_α and E_m) are (81.82, 82.38 kJ/mol.) and (21.81, 21.84) for ($\ln A_\alpha$ and $\ln A_m$) at $\alpha = 0.65$. It is clear from the above results that a good close between (E_α and E_m) and also between both ($\ln A_\alpha$ and $\ln A_m$), for each β, have been achieved for $Se_{77}Te_{20}Sb_3$ glass.

Fig. 6 shows the $g(\alpha)/g(0.5)$ reconstructed from the experimental data and according to the reaction model chosen (Avrami–Erofeev with the power exponent l/2, i.e. $g(\alpha) = [-\ln(1-\alpha)]^{1/n}$ with $n = 2$, model A2) at $\beta = 4$–30 K/min (solid line) for whole range of α, where $g(0.5)$ refers to $g(\alpha)$ at $\alpha = 0.5$. While, Fig. 7 shows the same plot for higher rates ($\beta = 35$–90 K/min), which the best reaction model chosen is A3/2 (Avrami–Erofeev with the power exponent 2/3, i.e. $g(\alpha) = [-\ln(1-\alpha)]^{1/n}$ with $n = 1.5$) that fits with the $g(\alpha)/g(0.5)$ reconstructed from the experimental data for a range of $\alpha = 0.05$–0.95 (solid line).

A confirmation about the best model chosen to describe crystallization process of the present glassy $Se_{77}Te_{20}Sb_3$ is to calculate the local Avrami exponent, $n(\alpha)$, which its value gave information about the nucleation and growth process. Lu et al. [7] deduced new equation in order to calculate local Avrami exponent for non-isothermal experiments, which is expressed as follows:

$$n(\alpha) = \frac{-R\,\partial \ln[-\ln(1-\alpha)]}{E_\alpha\,\partial(1/T)} \qquad (10)$$

Under the non-isothermal conditions, Avrami exponent can be obtained by plotting $\ln[-\ln(1-\alpha)]$ against $1000/T$ for different heating rates, as shown in Fig. 8. The slope of each line, shown in Fig. 8, is equal to $n(\alpha)E_\alpha/R$. By using the value of activation energy of crystallization, E_α, evaluated by KAS method in Eq. (10), the local Avrami exponent, $n(\alpha)$, could be calculated. In this work, the sample is pre-annealed for a period of time before each experimental run at temperature below the glass transition temperature (T_g), the condition of site saturation could be fulfilled to get an information about the growth mechanism separately from the nucleation process.

Fig. 9 shows the local Avrami exponent, $n(\alpha)$, as a function of the volume of the crystallization fraction, α, for $\beta = 4$–30 K/min. While, Fig. 10 shows the same plot for higher heating rates ($\beta = 35$–90 K/min). The range of α shown in these figures, $\alpha = 0.2$–0.8, is according to the linear part shown in Fig. 8.

According to the results obtained from Figs. 9 and 10, the $n(\alpha)$ is increased with increasing α for each heating rate. In addition, the maximum change in the values of n, for any heating rate shown in Figs. 9 and 10, is less than half. On the other hand, the values of $n(\alpha)$ decreased with increasing the heating rate for each α. As shown in Fig. 11, the dependence of $n(\alpha)$ on β (for $\alpha = 0.2$, 0.5 and 0.8) indicates that two heating rate regions can be identified. The first one for a heating rate from 4 to 30 K/min, the second one is for a higher heating rate (35–90 K/min), for all values of α.

It is clear from Fig. 9 that the minimum value of n is about 1.6 (at $\alpha = 0.2$ for $\beta = 30$ K/min) and its maximum value is about 2.48 (at $\alpha = 0.8$ for $\beta = 4$ K/min). The fraction of the minimum n (=0.6) is higher than 0.5, while, the fraction of the maximum n (=0.48) is less than 0.5. It seems from the range of n (1.6–2.48), that the average value of n is about (2.04), which indicates one mechanism (two-

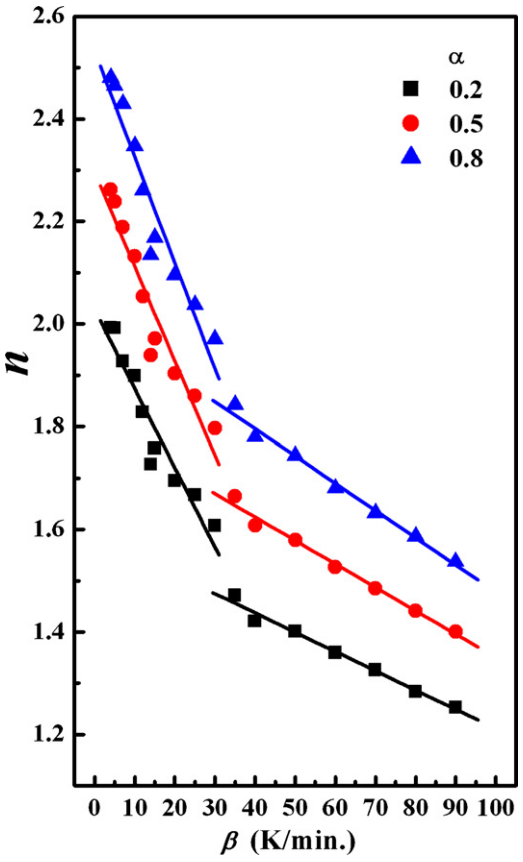

Fig. 11. The dependence of local Avrami exponent, $n(\alpha)$, on the heating rate, β, for the volume of the crystallization fraction, $\alpha = 0.2$, 0.5 and 0.8. The solid lines are guide for the eye.

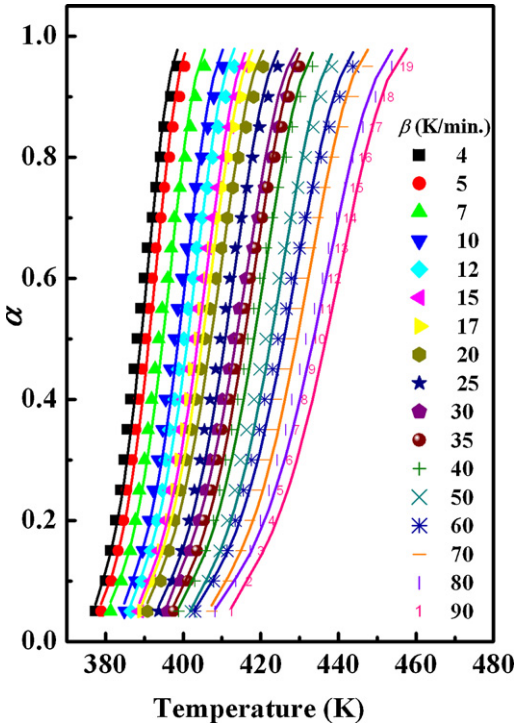

Fig. 12. The experimental and the reconstructed for the volume of the crystallization fraction, α, against temperature T for β = 4–90 K/min.

dimensional growth) may occur in the range of heating rates from 4 to 30 K/min. This result agrees well with the value of n obtained according to model A2, see Fig. 6. While, the minimum value of n is about 1.25 (at α = 0.2 for β = 90 K/min) and its maximum value is about 1.84 (at α = 0.8 for β = 35 K/min). This result indicates that two mechanisms (one- and two-dimensional growth) are working simultaneously during the amorphous–crystalline transformation of the glassy $Se_{77}Te_{20}Sb_3$ for higher range of heating rates. From this range of n (1.25–1.84), the average value of n (1.55) is agree with the value obtained according to the reaction model A3/2 shown in Fig. 7 for β = 35–90 K/min.

Another confirmation about the best values of kinetic parameters obtained is the comparison between the experimental and recalculated (α–T) curves. Fig. 12 shows comparatively the experimental data and reconstructed (α–T) curves using the kinetic parameters obtained for each heating rates. It is clear that, there is a good agreement between the experimental and the reconstructed (α–T) curves have been achieved.

From all the above results obtained one could conclude that the variation of the kinetic triplet (E_α, A_α, and $g(\alpha)$) are considered as a sign of the complex and multi-step mechanism. So, the transformation from amorphous to crystalline present in amorphous $Se_{77}Te_{20}Sb_3$ glass cannot be described by a single-step mechanism, but demonstrates complex multi-step involving several processes of growth with different activation energies and mechanisms.

4. Conclusions

The kinetic parameters of glassy $Se_{77}Te_{20}Sb_3$ under non-isothermal conditions are analyzed by the model-fitting and model-free approaches from a series of experiments at different constant heating rates (β = 4–90 K/min). The activation energy, E_α, was calculated by five different isoconversional methods (Vyazovkin, KAS, Starink, Tang and FWO) without previous assumption regarding the conversion model fulfilled by the reaction. The reaction model that well describe the crystallization process of the present glassy $Se_{77}Te_{20}Sb_3$ are model A2 (Avrami–Erofeev with n = 2) for β = 4–30 K/min and model A3/2 (Avrami–Erofeev with n = 1.5) for β = 35–90 K/min, for a whole range of α (0.05–0.95). The crystallization mechanisms examined using the local Avrami exponents indicate that one mechanism (two-dimensional growth) is responsible for the crystallization process for heating rates (4–30 K/min) and two mechanisms (one- and two-dimensional growth) are working simultaneously during the amorphous–crystalline transformation of glassy $Se_{77}Te_{20}Sb_3$ for higher heating rates (35–90 K/min). A good agreement between the experimental and the reconstructed (α–T) curves has been achieved. Finally, the transformation from amorphous to crystalline present in amorphous $Se_{77}Te_{20}Sb_3$ glass cannot be described by a single-step mechanism but the transformation demonstrates complex multi-step involving several processes of growth with different activation energies and mechanisms.

Acknowledgement

I would like to thank Dr. A.A. Abu Sehly, Physics Department, Faculty of Science, Taibah University, Madina, Saudi Arabia for supplying the specimens.

References

[1] H.E. Kissinger, Anal. Chem. 29 (1957) 1702.
[2] J.H. Flynn, L.A. Wall, J. Res. Natl. Bur. Stand. Sect. A 70 (1966) 487.
[3] T. Ozawa, Bull. Chem. Soc. Jpn. 38 (1965) 1881.
[4] T. Akahira, T. Sunose, Res. Rep. Chiba Inst. Technol. 16 (1971) 22.
[5] S. Vyazovkin, I. Dranca, Macromol. Chem. Phys. 207 (2006) 20.
[6] M.J. Starink, J. Mater. Sci. 42 (2007) 483.
[7] W. Lu, B. Yan, W. Huang, J. Non-Cryst. Solids 351 (2005) 3320.
[8] A.A. Elabbar, M. Abu El-Oyoun, A.A. Abu-Sehly, S.N. Alamri, J. Phys. Chem. Solids 69 (2008) 2527.
[9] A.A. Joraid, A.A. Abu-Sehly, M. Abu El-Oyoun, S.N. Alamri, Thermochim. Acta 470 (2008) 98.
[10] B. Guo, Q. Zou, Y. Lei, M. Du, M. Liu, D. Jia, Thermochim. Acta 484 (2009) 48.
[11] J.L. Cadenas-Leal, J. Vazquez, D.G. Barreda, P.L. Lopez-Alemany, P. Villares, R. Jiménez-Garay, Thermochim. Acta 484 (2009) 70.
[12] T. Spassov, St. Todorova, V. Petkov, J. Non-Cryst. Solids 355 (2009) 1.
[13] M. Erceg, T. Kovacic, I. Klaric, Thermochim. Acta 485 (2009) 26.
[14] F. Liu, S.J. Song, J.F. Xu, J. Wang, Acta Mater. 56 (2008) 6003.
[15] J.X. Lin, C.Y. Wang, Y.Y. Zheng, Comput. Chem. Eng. 32 (2008) 3023.
[16] H.C. Yang, H.C. Eun, Y.Z. Cho, H.S. Lee, I.T. Kim, Thermochim. Acta 484 (2009) 77.
[17] P. Karthik Reddy, A.C.K. Chowlu, A.K. Ghoshal, Appl. Catal. A: Gen. 351 (2008) 195.
[18] Z. Huang, J. Li, Q. Rao, Y. Zhou, J. Non-Cryst. Solids 355 (2009) 154.
[19] A. Inoue, X.M. Wang, Acta Mater. 48 (2000) 1383.
[20] X.L. Li, X.F. Bian, L.N. Hu, Y.Q. Wu, J.Y. Zhang, J. Alloys Compd. 439 (2007) 87.
[21] H. Men, W.T. Kim, D.H. Kim, Mater. Trans. 44 (2003) 1647.
[22] N.S. Saxena, J. Non-Cryst. Solids 345&346 (2004) 161.
[23] A.S. Soltan, Physica B 307 (2001) 78.
[24] A.H. Moharram, M. Abu El-Oyoun, A.A. Abu-Sehly, J. Phys. D: Appl. Phys. 34 (2001) 2541.
[25] A.A. Joraid, Thermochim. Acta 456 (2007) 1.
[26] B. Jankovic, J. Phys. Chem. Solids 68 (2007) 2233.
[27] S. Vyazovkin, C.A. Wight, Thermochim. Acta 340–341 (1999) 53.
[28] J. Bonastre, L. Escoda, J. Saurina, J.J. Sunol, J.D. Santos, M.L. Sanchez, B. Hernando, J. Non-Cryst. Solids 354 (2008) 5126.
[29] S. Vyazovkin, J. Comput. Chem. 22 (2001) 178.
[30] H.E. Kissinger, J. Res. Nat. Bur. Stand. 57 (1956) 217.
[31] M.J. Starink, Thermochim. Acta 404 (2003) 163.
[32] W. Tang, Y. Liu, H. Zhang, C. Wang, Thermochim. Acta 408 (2003) 39.
[33] B. Saha, A.K. Maiti, A.K. Ghoshal, Thermochim. Acta 444 (2006) 50.
[34] B. Jankovic, B. Adnadevic, J. Jovanovic, Thermochim. Acta 452 (2007) 106.
[35] B. Jankovic, J. Chem. Eng. 139 (2008) 128.
[36] P. Budrugeac, A.L. Petre, E. Segal, J. Comput. Chem. 47 (1996) 123.
[37] N. Sbirrazzuoli, Y. Girault, E. Elegant, Thermochim. Acta 293 (1997) 25.
[38] P. Budrugeac, D. Homentcovschi, E. Segal, Therm. Anal. Calorim. 66 (2001) 557.
[39] S. Vyazovkin, J. Therm. Anal. Calorim. 83 (2006) 45.
[40] S. Vyazovkin, Anal. Chem. 74 (2002) 2749.
[41] S. Vyazovkin, C.A. Wight, J. Phys. Chem. A 101 (1997) 8279.
[42] J.A. Kennedy, S.M. Clark, Thermochim. Acta 307 (1997) 27.
[43] S. Vyazovkin, W. Linert, Chem. Phys. 193 (1995) 109.
[44] S. Vyazovkin, A.I. Lesnikovich, Thermochim. Acta 128 (1988) 297.